International Journal of Heat and Mass Transfer 51 (2008) 5522–5533

Contents lists available at ScienceDirect

International Journal of Heat and Mass Transfer

journal homepage: www.elsevier.com/locate/ijhmt

A multi-segmented human bioheat model for transient and asymmetric radiative environments

M. Al-Othmani [a], N. Ghaddar [a,*], K. Ghali [b]

[a] Department of Mechanical Engineering, Faculty of Engineering and Architecture, American University of Beirut, P.O. Box 11-0236, Riad El Solh, Beirut 1107 2020, Lebanon
[b] Department of Mechanical Engineering, Beirut Arab University, Beirut, Lebanon

ARTICLE INFO

Article history:
Received 26 October 2007
Received in revised form 4 April 2008
Available online 9 June 2008

Keywords:
Multi-segment human bioheat model
Spatially non-uniform radiative environments
Circumferential skin temperature
Skin blood perfusion rates

ABSTRACT

This paper aims to improve the Salloum et al. multi-node multi-segmented model [M. Salloum, N. Ghaddar, K. Ghali, A new transient bio-heat model of the human body and its integration to clothing models, Int. J. Therm. Sci. 46 (4) (2007) 371–384] to accurately predict the circumferential skin temperature variation of nude and clothed human body segments when subject to complex transient and spatially non-uniform radiative environments. The passive bioheat model segments the body into the 15 cylindrical segments. Each body segment is divided into one core node, six angular skin nodes, one artery blood node, and one vein blood node. The model calculates the blood circulation using the Avolio model [A.P. Avolio, Multi-branched model of the human arterial system, Med. Biol. Eng. Comp. 18 (1980) 709–718] for arteries and arterioles up to 2 mm in diameter and the Olufsen et al., semi-analytical model [M.S. Olufsen, C.S. Peskin, W.Y. Kim, E.M. Pedersen, A. Nadim, J. Larsen, Numerical simulation and experimental validation of blood flow in arteries with structured tree outflow conditions, Ann. Biomed. Eng. 28 (11) (2000) 1281–1299] for small arteries and arterioles up to a minimum diameter of 0.3 mm; thus improving prediction of blood perfusion rates in the skin. Unsteady bioheat equations are simultaneously solved for the nodes of each body segment to predict the skin, tympanic, and core temperatures, sweat rates, and the dry and latent heat losses. The nude body thermal model is integrated to a clothing model that takes into consideration the moisture adsorption by the fibers to predict heat and mass diffusion through the clothing layers. The clothing layer is divided into six parts that are aligned to the skin sub-nodes for each clothed segment. The local and mean skin temperature can then be estimated in response to non-uniform environments.

The nude body and the clothed model predictions were compared with published experimental data at a variety of ambient conditions, non-uniform conditions and activity levels. The current model agreed well with experimental data during transitions from hot to cold, dry to humid environments, and in asymmetric radiative environments. Both the nude and clothed human models have an accuracy of less than 6% for the whole-body heat gains or losses; the nude human model has an accuracy of ±0.35 °C for skin temperature values.

1. Introduction

Non-uniform and transient environments are typically encountered in buildings and in situations where exposure to high or low temperature surfaces or sources is part of the job of the person. For example, fire fighters, astronauts, and drivers are frequently exposed while in duty to thermal stresses induced by overheating or overcooling of local areas of the body. Knowledge of human thermal response to non-uniform and disparate environments even over short periods of time is important to assess physiologic performance, comfort, and safety.

Numerous human bioheat models have been developed in the past few decades with the aim of predicting human thermal responses and body heat loss in steady and uniform thermal environments at various activity levels to relate the human thermal state and thermal sensation to comfort. The model development went into stages starting from analytical bioheat models of Pennes [4] and Weinbaum and Jiji [5], followed by two-node models of core and skin heat balances led by work of Gagge [6], to multi-node single-segment and multi-segment models of the human body and its thermoregulatory responses that were initially developed by Stolwijk [7,8], Wissler [9], and Wyndham and Atkins [10]. Subsequent bioheat models of Huizenga and Hui [11] (known as the Berkeley model), Tanabe and Kobayashi model [12], and Fiala et al., [13], and Salloum et al. [1], (known as the AUB model) were extensions and improvements of multi-node multi-segment

* Corresponding author. Tel.: +961 1 3500000x3594; fax: +961 1 744462.
E-mail address: farah@aub.edu.lb (N. Ghaddar).

0017-9310/$ - see front matter © 2008 Elsevier Ltd. All rights reserved.
doi:10.1016/j.ijheatmasstransfer.2008.04.017

Nomenclature

A	area (m^2)
AUB	American University of Beirut
C	thermal capacitance (J/K)
c	specific heat (J/kg K)
$F_{ski\rightarrow j}$	view factor between skin sector i and surface j
$h(t)$	pulsating blood flow convective heat transfer coefficient (W/m^2 K)
h_c	convective heat transfer coefficient (W/K m^2)
h_e	evaporative transfer coefficient (W/kPa m^2)
h_{fg}	water latent heat of vaporization (J/kg)
h_{mean}	mean non-pulsating blood flow convection coefficient (W/m^2 K)
h_{rij}	radiative heat transfer coefficient between surfaces i and j
I_{sk}	skin evaporative resistance, (m^2 kPa/W)
$I_{a\text{-}sk}$	evaporative resistance of air layer adjacent (m^2 kPa/W)
K	conductance (W/K).
L_n	length of the body segment n
M	metabolic rate (W)
M_{total}	total metabolic rate (W)
W	external work (W)
$\dot{m}$	blood mass flow rate (kg/s)
m_{sw}	sweat rate (kg/s)
P	vapor pressure (kPa).
$P_{sat,sk}$	saturation vapor pressure at the skin temperature (kPa)
$Q_{rad,i}$	heat transfer by radiation (W)
Q_s	heat of adsorption (J/kg)
r	radius (m)
R	local fabric regain (kg of adsorbed H_2O/kg fiber)
R_d	combined air-clothing layer dry resistance (m^2 K/W)
$R_{d,fab}$	fabric dry resistance (m^2 K/W)
R_e	combined air-clothing layer evaporative resistance (m^2 kPa/W)
$R_{e,fab}$	fabric evaporative resistance (m^2 kPa/W)
t	time (s)
$th_{sk,i}$	thickness of skin node sector (m)
T	temperature (°C)

Greek symbols

α	skin absorptivity
ΔT_{pr}	radiative temperature asymmetry
δ_i	non-uniformity in skin temperature of segment i (K)
ε	surface emissivity
θ	angular coordinate
ρ	density (kg/m^3)
σ	Stefan Boltzmann constant

Subscripts

a	artery
bl	blood
bl,a	artery blood
bl,v	vein blood
C	convective
co	constricted
cr	core
cr–sk	between core and skin
dil	dilated
fab	fabric
i	skin node sector index (i = 1–6)
mean	mean
n	segment number
perfusion, total: total blood perfusionr	
	radiative
resp	respiratory
sk, skin	skin
s	sorptive
shiv	shivering
v	vein

Greek subscript

∞	ambient

models [6–9] as more experimental data on human physiology and human circulatory system became available. The multi-segmental bioheat models were based on theories of physiology, thermodynamics and transport processes for the prediction of thermal behavior of either the entire human body or a part of it [1,11–15]. More complex 3D finite element bioheat model was also developed by Smith [16] (known as the KSU model) but the model is computationally prohibitive for integration with space thermal models to predict the human thermal comfort state.

Few of the developed multi-segmented bioheat simulation models dealt with spatially non-uniform and time varying environments [14,15,17]. Latest thermal comfort models for transient and non-uniform thermal environments are moving towards relating global comfort sensation to mean and local skin temperatures, core temperature, and local heat transfer [17–20]. There is a need to develop accurate and computationally effective bioheat models of nude and clothed human that are capable of predicting circumferential skin temperature variation in response to a transient non-uniform environment. The multi-node multi-segment AUB (American University of Beirut) model [1] used accurate and realistic representation of the arterial system including blood flow pulsation. The AUB model was based on exact anatomical data of the human body [2] and real dimensions and anatomic positions of the arteries in the body. The model used the heart rate as input and calculated blood perfusion in the core tissue based on the pulsating arterial system model. The AUB model, however, was not sensitive to angular variation in skin temperature. The model is in need of improvement before it can be used in non-uniform environment applications [21–23].

The aim of this work is to extend the AUB bioheat model for the nude and clothed human body to transient non-uniform environment applications by accounting for heat exchanges in angular directions of each of the body segments and to further improve the model predictions of blood perfusion rate in the skin under non-uniform angular heat exchanges with environment. The skin nodes of clothed segments of the human body will be associated with a simple two-dimensional multi-clothing layer model to predict skin local temperature and asymmetric heat exchange through clothing layers. The improved model will be validated against published experimental and simulation data of thermal response in transient uniform and non-uniform environment.

2. Improvemnets to AUB bioheat model

The AUB bioheat has undergone two major improvements. The first is related to modeling asymmetry in each segment of the human thermal model and the second is related to improving blood circulatory model for prediction of perfusion flow rates in the skin nodes. The following sections outline the improvement followed by energy balance integral equations for all the nodes and the clothing.

2.1. Modeling passive system asymmetry (two-dimensional heat conduction)

The AUB multi-segmented bioheat model is extended to two-dimensions in each segment to represent heat transfer in angular direction in addition to the radial direction. Salloum et al. [1] divided the human body into 15 segments: head, chest, upper arms, forearms, hands, thighs, calves, and feet. In this work, each of the 15 nude body cylindrical segments is composed of six skin nodes instead of the one node in the AUB model, one core node, an artery node, and a vein node that sum up into nine nodes as shown in Fig. 1. Fiala et al. [13] used three angular skin nodes in their dynamic model while the current model is using six nodes. Asymmetry is well captured when the skin is decomposed to six angular equal parts as was reported by Mungcharoen and Wissler [24] and Iyoho et al., [25]. The clothing layer is divided into six parts that are parallel to the skin nodes as shown in Fig. 1. The clothing model is based on radial heat and mass diffusion through the fabric that accounts for moisture absorption by the fibers. The heat generated by the human body is enhanced or dissipated to the environment through radiation, convection, and evaporation to maintain the core temperature within a narrow range.

2.2. View factors determination

The radiative heat exchange of the person and surrounding non-uniform surfaces necessitates accurate calculation of view factors between surrounding surfaces and various body elements. These calculations, performed over an irregular human body shape and arbitrary position of body parts is computationally expensive, particularly when body surfaces are close to a radiating wall and some body limbs shadow other parts of the body from radiating surfaces. The Fanger graphical method [26] cannot be used since it is for whole-body view factors rather than individual segments. The view factor between any two surfaces in space is calculated using a Gaussian integration technique for any surface dimension, and orientation. In this work, an improved and rapid method is developed using the analytical model of Gross et al. [27] and Krishnaprakas [28] for simple surface geometries and the Ghaddar et al. [29] computer model for cylindrical surfaces. The Ghaddar et al. [29] model was based on a detailed finite element method for performing the Gaussian integration and using the shadowing algorithm of He [30] to accurately compute shape factors between surrounding walls and each segment skin/clothing node for any surface orientation or shape. A comparison between view factors obtained in this model and the Fanger results for a standing and a seated person facing a vertical wall has shown good performance of the present model.

2.3. Circulatory system model

In any body element, the blood exiting the arteries and flowing into the capillaries is divided into blood flowing in the core that exchanges heat by perfusion in the core and blood flowing into the different skin parts and exchanges heat by perfusion in the skin after crossing the core tissue. Fig. 2 shows a plot of (a) the blood flow in arteries and veins and (b) a representation of core, skin, artery blood, and vein blood nodes and heat exchanges between the nodes for a body segment and with adjacent segments. The blood entering a segment (from an artery) will split into a perfusion flow (including the skin blood flow) in the considered segment and a blood flow entering the adjacent segment. The opposite takes place in the veins for the same segment (see Fig. 2b). For peripheral

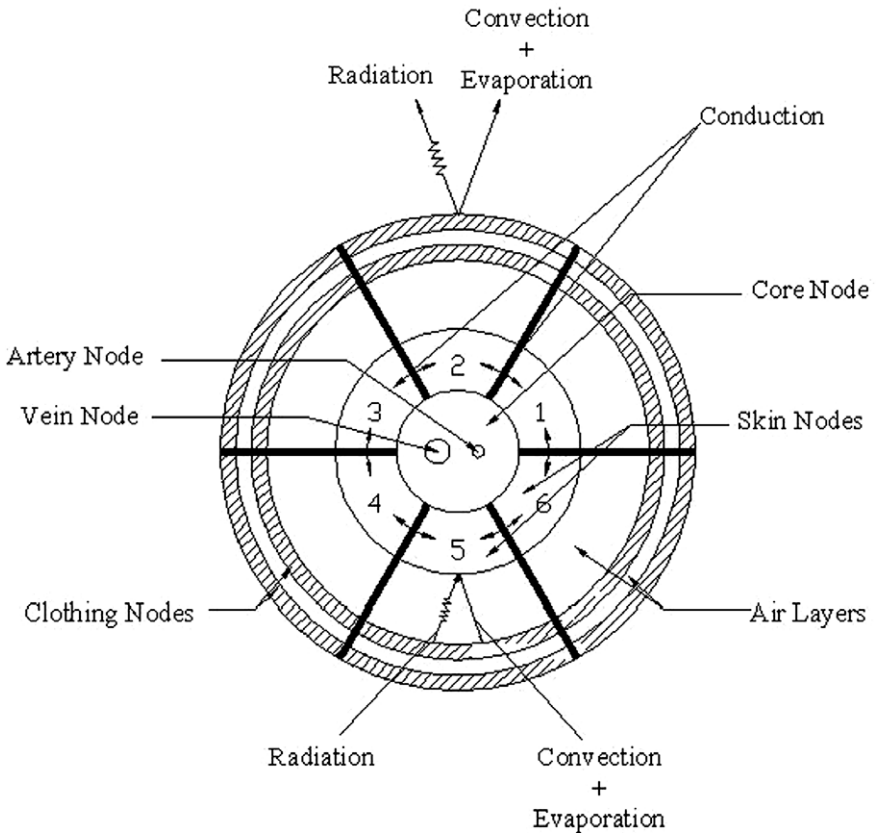

Fig. 1. Schematic of segmental nodes of core, skin, artery, vein, and clothing.

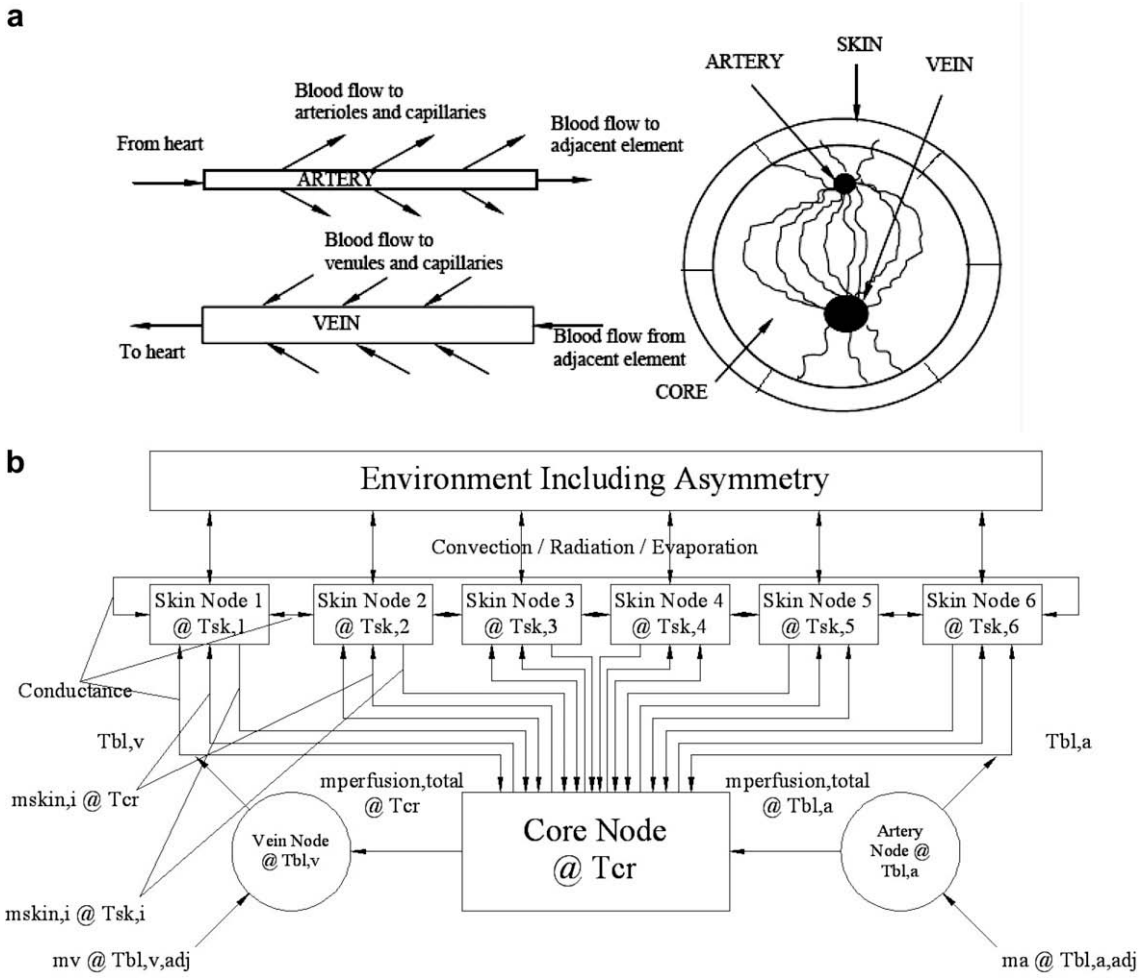

Fig. 2. Representation of (a) blood flow in arteries and veins and (b) core, skin, artery and vein nodes and their interaction for a nude body segment.

segments (head, hand and foot), the blood entering rate is equal to the blood perfusion rate and the blood exiting rate.

The purpose of the explicit blood circulation representation used in the AUB bioheat model is to predict the blood flow and pressure at any position along the larger systemic arteries defined by Avolio [2]. This was done in this work by using the nonlinear formulation of the Avolio model [2] for larger arteries and by using the model developed by Olufsen et al. [3] and Olufsen [31,32] for smaller arteries. The arteries are represented by uniform thin-walled elastic[1] tubes with realistic arterial dimensions and wall properties. The human circulatory system was represented by 128 arteries with lengths drawn proportional to actual vessel length while each artery vessel is identified by a branch number. The details of length and diameter of each cylindrical vessel can be found in Avolio's work [2]. The minimum artery diameter in the Avolio model [2] was 1.2 mm and the peripheral beds were considered as pure resistors. The principal variables of an arterial segment are the characteristic impedance and the propagation constant. The expressions of the complex characteristic impedance and propagation constant for one artery can be found in the work of Avolio as a function of the blood density, the pulsating frequency, wall thickness, wall Young modulus of elasticity, and the Poisson's ratio of the arterial wall [2]. The problem when using a simple model for the peripheral beds such as pure resistor model [33] or Windkessel model [34,35] is that these models are lumped and they cannot include wave propagation effects in the part of the arterial system that they model. The idea adopted in this work for modeling of the blood circulatory system follows the Avolio model for the large artery tree, while small structured artery trees at each terminal follow the Olufson model [31,32]. In the model, the inflow boundary conditions are calculated by representing the heart outflow using Fourier series and the outflow boundary conditions are calculated using the small arteries model [3,31,32]. Regarding the small artery model, it is sufficient to calculate the impedance recursively in order to reach the large arteries. The heart outflow is the input boundary condition to the Avolio tree [36]. A recursive system is used to generate the arterial tree and terminates at a minimum radius that was selected to be 0.03 mm. The distribution of Avolio arteries and inlet and outlet arteries of each segment, and basic body parameters at basal metabolic generation can be found in Salloum et al. work [1].

3. Mathematical model

3.1. Energy balance integral equations

The circulatory system model is used to predict the blood flow in the arteries and veins and perfusion rates in the core while the skin perfusion blood flow is calculated based on empirical and experimental correlations reported by Fu [37]. The perfusion blood flow rate ($\dot{m}_{\text{perfusion}}$) through the capillaries is calculated by

[1] The characteristics impedance of the artery flow in Avolio model is corrected to include the effect of the wall Young modulus, wall thickness, and Poisson ratio in the propagation constant and wave velocity.

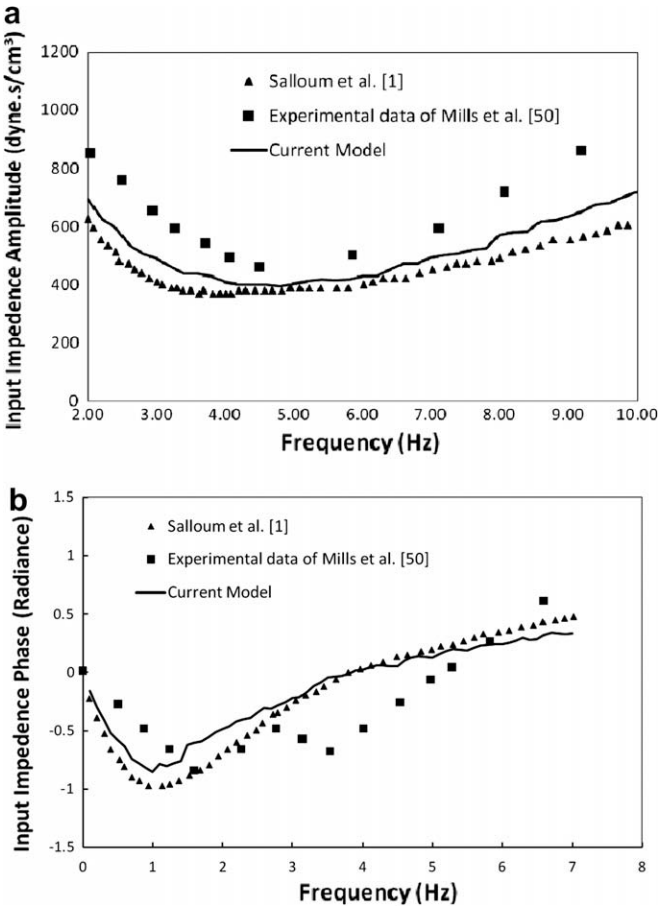

Fig. 3. Plots of (a) the input impedance amplitude and (b) the input impedance phase as function of the pulsation frequency for the current model and the published data of Mills et al. [50], and model results of Salloum et al. [1].

Table 1
Calculated basal perfusion blood flow rate of the current model and the published data of Gordon et al. [39], Ganong [51] and Salloum et al. [1]

Human body segment	Experimental perfusion flow rate [39,51] (cm^3/h)	Salloum et al. [1] model perfusion flow rate (cm^3/h)	Current model perfusion flow rate (cm^3/h)
Head	56,526	58,829	57,758
Chest	198,164	194,352	194,677
Upper arm	3852	3577	3612
Forearm	2152	2266	2224
Hand	1378	1502	1443
Thigh	6196	6520	6391
Calf	2741	2531	2551
Foot	1339	1288	1309
Total cardiac ‘output	290,006	288,549	287,494

subtracting the exiting flow from the entering blood flow of the considered segment. Larger arteries, veins, and arterioles are assumed to exchange heat by convection with the core of the body. The venules located in the tissue (skin and core) exchange heat between the core and the skin. These small vessels play a major role in thermoregulation where the skin blood flow varies as a function of the core and skin temperatures [16]. The information is then used to update the energy balances of each body segment.

The core energy balance of the AUB model of a body segment n is modified to accommodate heat exchanges between the core node and the six skin nodes as follows:

$$C_{cr}\frac{\partial T_{cr}}{\partial t} = \sum_{i=1}^{6} K_{n,i}(T_{sk,i} - T_{cr}) - \left[\sum_{\substack{\text{arteries}\\ \text{arterioles}}} h(t)\cdot A_a\right]\cdot[T_{cr} - T_{bl,a}] - \left[\sum_{\text{veins}} h_{mean}\cdot A_v\right]\cdot[T_{cr} - T_{bl,v}] + \dot{m}_{perfusion,total}\cdot c_{bl}\cdot(T_{bl,a} - T_{cr}) + \sum_{i=1}^{6}\dot{m}_{skin,i}\cdot c_{bl}\cdot(T_{sk,i} - T_{cr}) + M_{cr} + M_{shiv} - W - \alpha\cdot Q_{resp} \quad (1)$$

where C_{cr} is the thermal capacitance of the segment core, α is equal to unity for the chest and zero for all other elements, W is the mechanical work generated by the body, Q_{res} is the heat dissipated by respiration calculated based on the known ASHRAE correlations [30], where $K_{n,i}$ (W/°C) is the skin sector i to core conductance in segment n, The values of K are based on the correlations of Havenith [38] and the physiological data of Gordon [39]. $h(t)$ is the pulsating heat convection coefficient of the blood flow in arteries, h_{mean} is the mean non-pulsating convection coefficient of blood flow in veins which have twice the arteries diameter, $\dot{m}_{perfusion,total}$ is the total perfusion rate of blood entering the core; $\dot{m}_{skin,i}$ is the skin perfusion blood flow for skin node i, A_a or A_v is the surface area of the blood vessel, M_{cr} is the basal metabolic heat generated in each segment [16], and M_{shiv} is the segmental thermoregulatory metabolic rate generated by shivering. The respiration heat loss by convection and evaporation is considered to be associated to the chest where most of the dissipation occurs [12,16]. The heat dissipation by respiration in the head segment is negligible compared to the total heat dissipation of the head. Bioheat models of Smith [16] and Tanabe et al. [12] used the same assumption. The blood specific heat c_{bl} is taken as 4000 J/kg K.

The term on the left-hand side of Eq. (1) is the rate of accumulation of thermal energy per unit volume due to the changing temperature of core tissue. The first five terms on the right hand side of Eq. (1) represent: the heat exchange between the core node and skin nodes by conduction; the heat exchange between the core node and the arteries by convection; the heat exchange with veins by convection; the net heat flow associated with perfusion blood flow through capillaries entering the core at the arteries blood temperature and leaving at the core temperature [9,40,41]; and the net heat exchange associated with skin perfusion blood flow rates, $\dot{m}_{skin,i}$, between the skin nodes and the core node. The heat transfer coefficient $h(t)$ is obtained from isothermal quasi-steady wall correlation at $T_{bl,a}$ at the instantaneous pulsating artery flow velocities obtained from the circulatory model. The summation of the product of the arteries and arterioles surface areas with their corresponding pulsating heat transfer coefficients ($\sum_{arteries} h(t)\cdot A_a$) is performed over all the artery branches in the segment under consideration. Similarly, the summation of the product of the veins and venules surface areas with their corresponding mean convection coefficient is done for all the veins and venules of the segment under consideration. The model formulation assumes complete thermal equilibrium between blood and tissue [1] for all body parts meaning that the blood exiting the core node and entering the vein node is at core temperature. The thermal equilibrium assumption is valid because the blood flow through the core tissue is very slow and the core and blood system can be likened to a heat exchanger with a very high heat transfer area, area/volume ≈ 5000, as calculated from Milnor’s data [42]. This large heat transfer area makes the outlet blood temperature equal to the core temperature.

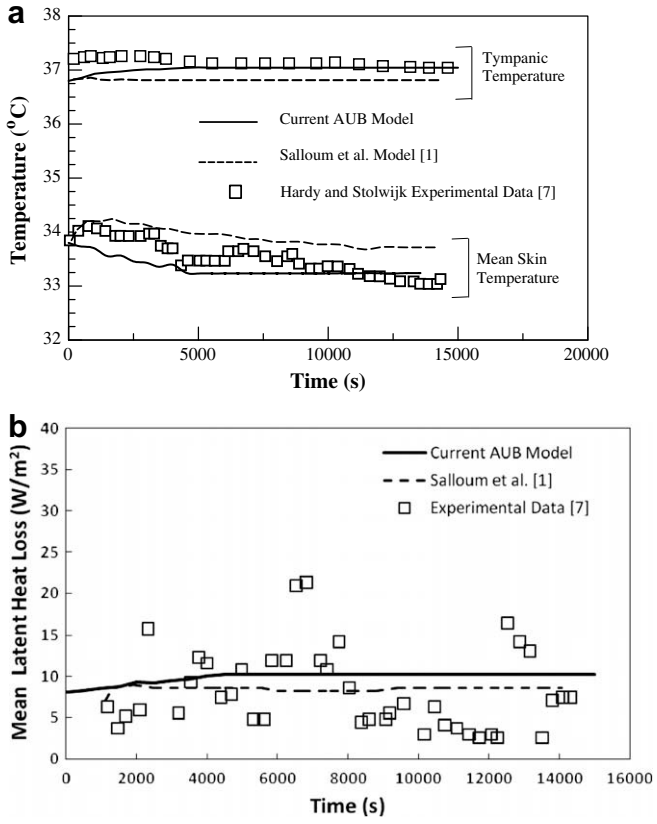

Fig. 4. The simulated results of the modified current AUB model of (a) tympanic and body mean skin temperature, and (b) latent heat loss as a function of time in addition to the reported experimental data of Hardy and Stolwijk [7] and simulation data of AUB model [1] at the same conditions of the experiment.

The arteries node energy balance is given by

$$C_{\mathrm{bl,a}} \cdot \frac{\mathrm{d}T_{\mathrm{bl,a}}}{\mathrm{d}t} = -\left[\sum_{\substack{\text{arteries}\\ \text{arterioles}}} h(t) \cdot A_{\mathrm{a}}\right] \cdot [T_{\mathrm{bl},a} - T_{\mathrm{cr}}] + \dot{m}_{\mathrm{a}} \cdot c_{\mathrm{bl}} \cdot (T_{\mathrm{bl},a,\mathrm{adjacent}} - T_{\mathrm{bl},a}) \quad (2)$$

where $\dot{m}_{\mathrm{a}}$ is the mass flow rate of blood entering the considered part through the inlet artery, and $\dot{m}_{\mathrm{a}}$ is assumed to change with time within one period of pulsation like the cardiac ejection waveform. The first term in the right hand side of Eq. (2) is the heat exchange by convection through the arteries walls and the second term is the net flow of heat through the inflow/outflow boundaries from one segment to the next (see Fig. 2a). Note that for the chest, there is no adjacent element, but the blood enters the chest from the heart at the same rate as the blood returning from the veins through the vena cava.

The vein node energy balance is given by

$$C_{\mathrm{bl,v}} \cdot \frac{\mathrm{d}T_{\mathrm{bl,v}}}{\mathrm{d}t} = -\left[\sum_{\text{veins}} h_{\mathrm{mean}} \cdot A_{\mathrm{v}}\right] \cdot [T_{\mathrm{bl,v}} - T_{\mathrm{cr}}] + \dot{m}_{\mathrm{v}} \cdot c_{\mathrm{bl}} \cdot (T_{\mathrm{bl,v,adjacent}} - T_{\mathrm{bl,v}}) + \dot{m}_{\mathrm{perfusion,total}} \cdot c_{\mathrm{bl}} \cdot (T_{\mathrm{cr}} - T_{\mathrm{bl,v}}) \quad (3)$$

where $\dot{m}_{\mathrm{v}}$ is the mass flow rate of blood entering the considered part through the inlet vein and $\dot{m}_{\mathrm{perfusion,total}}$ is the perfusion blood flow rate in the considered part where it enters the venous bed at core temperature and leaves at vein temperature.

The energy balance of a skin node i of a nude body segment n (n = 1 to 15) is given by

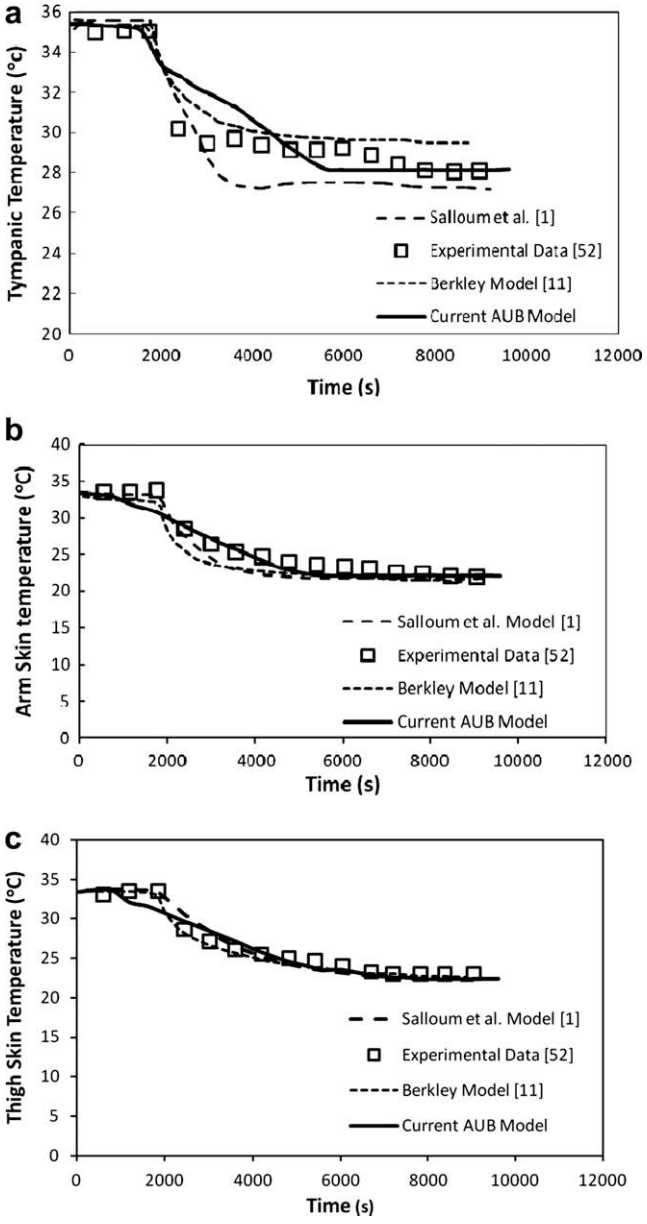

Fig. 5. A plot of the measured [52], simulated temperatures of Berkley Model [11] and Salloum et al. [1] and current model for a step change from 28 °C to 4.7 °C for (a) head skin temperature; (b) upper arm; and (c) thigh.

$$C_{\mathrm{sk}} \frac{\partial T_{\mathrm{sk},i}}{\partial t} = k_{\mathrm{sk},i} L_n \mathrm{th}_{\mathrm{sk},i} \frac{1}{r^2} \frac{\partial^2 T_{\mathrm{sk},i}}{\partial \theta^2} + K_{n,i}(T_{\mathrm{cr}} - T_{\mathrm{sk},i}) + \dot{m}_{\mathrm{skin},i} \cdot c_{\mathrm{bl}} \cdot (T_{\mathrm{cr}} - T_{\mathrm{sk},i}) + M_{\mathrm{sk},i} - \dot{Q}_{\mathrm{rad},i} - A_{\mathrm{sk},i} \cdot h_c \cdot (T_{\mathrm{sk},i} - T_{\infty}) - A_{\mathrm{sk},i} \cdot h_{\mathrm{e}} \cdot (P_{\mathrm{sk},i} - P_{\infty}) \quad (4)$$

where C_{sk} is the thermal capacitance of the skin node i (=1–6), k_{sk} is the skin thermal conductivity (W/m² K), θ is the angular skin coordinate of the segment cylinder, L is the segment length, and $\mathrm{th}_{\mathrm{sk},i}$ is the skin node thickness, $M_{\mathrm{sk},i}$ is the skin nodal metabolic rate equal to the segment overall metabolic rate divided by the total number of skin nodes in that segment. The skin nodal blood perfusion rate $\dot{m}_{\mathrm{skin},i}$ depends on the skin node temperature. A model is developed to estimate the angular distribution of the skin blood perfusion rates in response to non-uniformity in skin temperature $\delta_i = \left(T_{\mathrm{skin},i} - \left(\sum_{i=1}^{6} T_{\mathrm{skin},i}\right)/6\right)$. The total skin blood perfusion rate is divided into nodal values that are inversely proportional to the deviation of the individual skin node temperatures from the mean temperature of all the nodes in that segment.

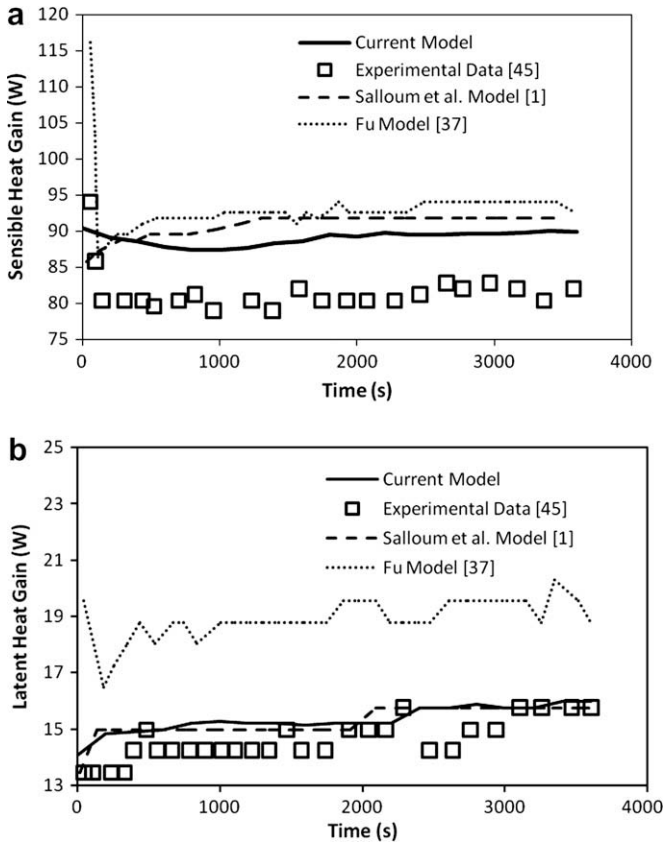

Fig. 6. A plot of measured data of Jones and Ogawa [45], the predicted values of current model and model results of Salloum et al. [1] and of Fu [37] of (a) sensible and (b) latent heat losses to the environment from the clothed human body (cotton, mixed cotton polyester, and polyester layers [1,45]).

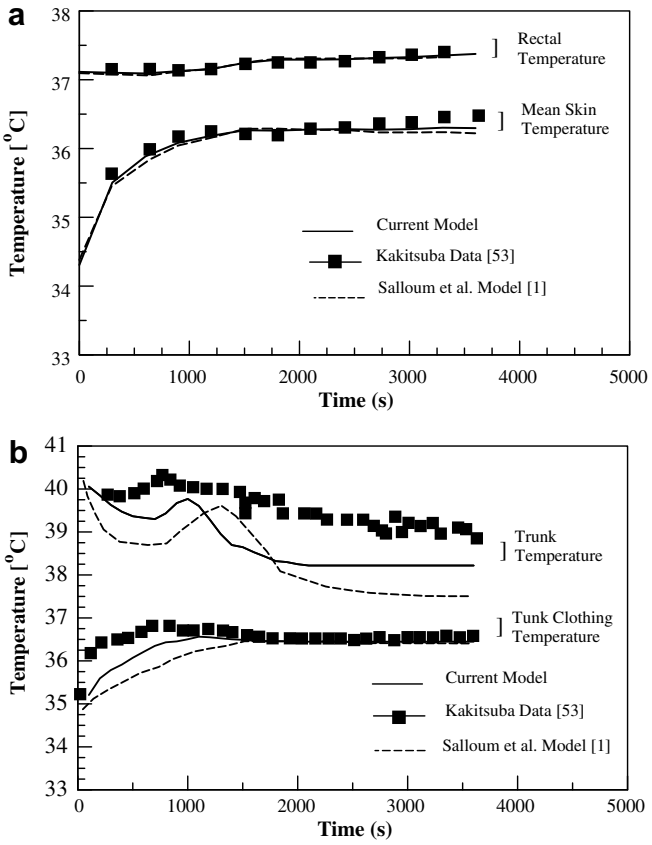

Fig. 7. A plot of the predicted (a) rectal and mean skin temperature and (b) the trunk skin and clothing temperatures by the current model, the Salloum et al. model [1] and by the experimental results of Kakitsuba [53].

$$\dot{m}_{\mathrm{skin},i} = \dot{m}_{\mathrm{skin,mean}}\left(1 + \frac{\delta_i}{\sum_i \max(0,\delta_i)}\right) \tag{5}$$

The last two terms of Eq. (4) represent the heat loss by convection and by evaporation from the skin to environment at temperature T_∞ and vapor pressure P_∞. The evaporation coefficient h_e is deduced from the convection coefficient h_c by Lewis relation of $h_e = 16.5h_c$ [44]. The external convection coefficients are determined using the correlation of Wang [43]. The skin vapor pressure, $P_{\mathrm{sk},i}$ is estimated using Jones model as [44]

$$P_{\mathrm{sk},i} = \frac{P_{\mathrm{sat,sk},i}\cdot I_{\mathrm{a\text{-}sk}} + P_\infty \cdot I_{\mathrm{sk}} + m_{\mathrm{sw},i}\cdot h_{\mathrm{fg}}\cdot I_{\mathrm{sk}}\cdot I_{\mathrm{a\text{-}sk}}}{I_{\mathrm{sk}} + I_{\mathrm{a\text{-}sk}}} \tag{6}$$

where I_{sk} is the evaporative resistance of the skin which is approximately 0.33 m^2 kPa/W for a well-hydrated person, $I_{\mathrm{a\text{-}sk}}$ is the evaporative resistance of the adjacent air layer in m^2 kPa/W and $m_{\mathrm{sw},i}$ is the local sweat rate (kg/m^2 s) [37]. The value of the skin vapor pressure is subject to the constraint that the vapor pressure calculated in Eq. (6) cannot exceed the saturation pressure at $T_{\mathrm{sk},i}$. Eq. (6) applies even if the sweat rate is zero. Jones and Ogawa [45] included in the boundary condition the accumulation of moisture on the skin and the evaporation of that moisture through a mass balance at the skin surface subject to the constraint that the accumulated moisture is less than 0.035 kg/m^2 based on the maximum sweat layer that can be sustained over the body which is about 35 μm [45].

The heat flux by radiation for skin node surface i is given by [46]

$$Q_{\mathrm{rad},i} = \varepsilon_{\mathrm{sk}}\sigma T_{\mathrm{sk},i}^4 - \alpha_i \sum_j \varepsilon_j \sigma T_j^4 F_{\mathrm{sk},i\to j} \tag{7}$$

where σ is the Stefan–Boltzmann constant, $\varepsilon_{\mathrm{sk}}$ is the skin surface emissivity, T is the surface temperature, α is the skin absorptivity assumed to be close to unity [13], and j is the surrounding surface index. $F_{\mathrm{sk},\,i\to j}$ is the view factor between the skin surface node area $A_{\mathrm{sk},i}$ and any other surface area A_j in the surroundings. The radiative flux can be written in terms of the radiative heat transfer coefficient h_{rij} as

$$Q_{\mathrm{rad},i} = \sum_j h_{rij}(T_{\mathrm{sk},i} - T_j)F_{\mathrm{sk},i\to j} \tag{8}$$

where the radiative heat transfer coefficient h_{rij} is given by [47]

$$h_{rij} = 4\sigma\varepsilon_{\mathrm{sk}}(T_{\mathrm{sk},i}^2 + T_j^2)(T_{\mathrm{sk},i} + T_j). \tag{9}$$

The reflected radiation from the surrounding surfaces is not included since the surfaces' emissivities of humans and walls of built-in environment are typically high ($\varepsilon = 0.9$–1) and satisfies Howell and Suryanarayana model condition for surface emittance at 0.9 and above [46].

The clothing cylindrical layers are divided into six sectors aligned with the skin nodes. Each clothing layer consists of a uniform porous material with constant evaporative and dry resistances and thermal properties. The heat flux in the clothing layers is considered unidirectional. A transient simplified mathematical model for clothing layers is adopted based on Jones [47] and Fu [37] models. The details of the simplified model can be found in references [1] and [47] and will not be repeated here, but data on the evaporative and dry resistances of fabrics are obtained from published data bases of Fu [37] and McCullough [48,49]. The obtained model is integrated with the nude body model through the skin node and can be manipulated for any number of clothing layers on any body segment [1]. The energy balance for the clothed skin node in Eq. (4) is modified to

$$C_{sk}\frac{\partial T_{sk,i}}{\partial t} = k_{sk,i}L_n \mathrm{th}_{sk,i}\frac{1}{r^2}\frac{\partial^2 T_{sk,i}}{\partial \theta^2} + K_i(T_{cr} - T_{sk,i}) + \dot{m}_{skin,i}\cdot c_{bl}\cdot(T_{cr} - T_{sk,i}) + M_{sk,i} - \frac{T_{sk,i} - T_{f,i,1}}{R_{d,airlayer,1}}\cdot A_{sk,i} - \frac{P_{sk,i} - P_{f,i,1}}{R_{e,airlayer,1}}\cdot A_{sk,i} \quad (10)$$

where $T_{f,i,1}$ is the fabric node i first layer temperature and $P_{f,i,1}$ is the fabric node i first layer vapor pressure, $R_{d,\text{air layer}}$ is the air layer dry resistance and $R_{e,\text{air layer}}$ is the air layer evaporative resistance. The dry and evaporative resistances of the air layer are reported by Jones [44] as

$$R_{d,\text{air layer}} = \frac{1}{h_r + k/\mathrm{th}_a}\left\{\begin{array}{l} h_r\ (\mathrm{W/m^2\,^\circ C}) \\ k = 24\ \mathrm{mm\,W/m^2\,^\circ C} \\ \mathrm{th}_a\ (\mathrm{mm})\text{air layer thickness}\end{array}\right\} \quad (11a)$$

$$R_{e,\text{air layer}} = a(1 - e^{-\mathrm{th}_{a/b}})\left\{\begin{array}{l} a = 0.034\ \mathrm{m^2\,kPa/W} \\ b = 15\ \mathrm{mm} \\ \mathrm{th}_a\ (\mathrm{mm})\ \text{air layer thickness}\end{array}\right\} \quad (11b)$$

3.2. Thermoregulatory control equations

The sudomotor and metabolic thermoregulatory functions follow the KSU model of Smith [16] and Fu [37] and will not be presented here. For vasomotor, the skin perfusion blood flow rate is evaluated from the thermal control equations which determine the thermal interaction between the skin and core by blood perfusion [1]. The same thermoregulatory control equations of Salloum et al. [1] are used in the current work except that the segmental mean skin temperature and the segmental skin blood perfusion rate are given respectively by

$$\dot{m}_{skin,perfusion} = \sum_{i=1}^{6}\dot{m}_{skin,i} \quad (12a)$$

$$T_{sk,mean} = \sum_{i=1}^{6} T_{sk,i}/6. \quad (12b)$$

4. Numerical method

A simulation program was developed. The input to the program consisted of the initial thermal state of the human body, the metabolic rate, the ambient conditions, the clothing properties, the clothing layers thicknesses, and the physiological and physical parameters inherent in the bioheat model of the human body. A fully explicit first order Euler-Forward integration scheme with a time step Δt of 0.02 s over the desired simulation period for sedentary activity was used to solve the energy balance equations of the human body nodes for any segment where the respiratory heat loss, blood flow rates, thermoregulatory responses and skin vapor pressure were calculated from previous time step. A smaller time step might be necessary at higher body activity level. The circumferential diffusion of heat in the skin node is discretized using central differencing. The view factors and the small arteries impedance are extracted from their own databases created previously. Numerical tests were for uniform time step sizes of 0.02 s, 0.01 s, and 0.005 s. The time step of 0.02 s was found to be of sufficient accuracy for our cases at relative error of less than 0.008% in values of blood flow rates compared to the lower time

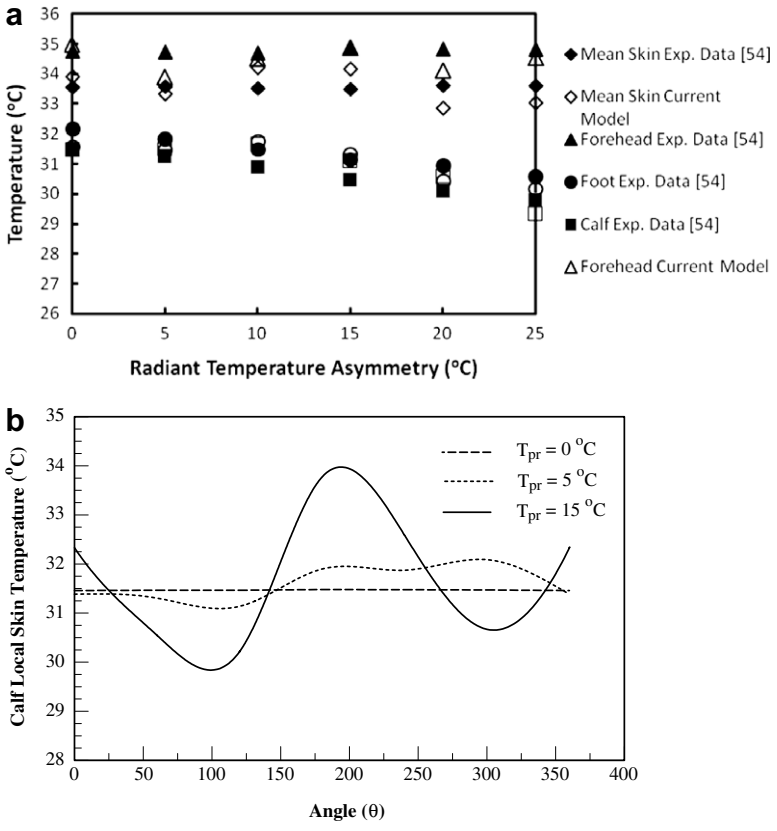

Fig. 8. A plot of (a) the reported measurements of Fanger et al. [54] and predicted values of current model of the skin temperature of the forehead, the calf, the foot, and the mean skin temperature as a function of radiant temperature asymmetry due to the hot ceiling and (b) the corresponding predictions of local temperature angular variation of the calf segment at radiant temperature asymmetry ΔT_{pr} of 0 °C, 5 °C, and 15 °C.

step and 10-4% in temperature. In transient simulations, a smaller time step size of 0.001 s was used at the times when sudden change in environment temperature or metabolic rate takes place. In transient simulations, suitable initial conditions were determined starting from the neutral conditions of T_{cr} = 36.8 °C, and T_{sk} = 33.7 °C to simulate a relatively long exposure to any preconditioning environment. Starting from uniform initial conditions will result with lower temperatures at extremities in steady environment. The obtained steady state values were then used as initial conditions for all other unsteady calculations of various node temperatures for all segments and the sensible and latent heat loss from the skin.

5. Results and discussions

5.1. Circulatory system model validation

The arterial circulation system is validated against published experimental data of Mills et al. [50] and model data of Salloum et al. [1] by comparing the frequency response of the input impedance (pressure to flow ratio) at the ascending aorta. The current simulation is run at frequency steps of 0.05 Hz. Fig. 3 shows (a) the input impedance amplitude and (b) the input impedance phase as function of the pulsation frequency for the current model and the published data. The modification on the circulatory model in the current step agrees better with experimental data of Mills at al [50] than the Salloum et al. model [1]. The better results of current model stem from the treatment of impedances of small artery tree model up to smaller arterioles diameter of 0.03 mm.

The arterial system is used to calculate blood flow rate to each body segment and the amount of blood perfusion rates that are carried from the core to the skin nodes. Table 1 presents the basal perfusion blood flow rate calculated using the current model, the published experimental perfusion flow rates of Gordon et al. [39] and Ganong [51] and the Salloum et al. model [1]. The modified circulatory model has improved predictive accuracy of blood perfusion in the hand from 9% in Salloum et al. [1] model to 4.5% in the current model. Similar improvements were also clear for the head, for arm, thigh, and foot.

5.2. Model validation

The multi-segmented 2D model is validated by comparing simulated skin, tympanic and rectal temperatures with published experimental [7,20,23] and simulation data of other nodal multi-segmented [1] for steady and transient uniform and non-uniform environment for a variety of activity levels.

5.3. Uniform environment

For a sedentary human condition, Hardy and Stolwijk reported experimental data for the mean skin temperature for resting human subjects who wore only shorts [7] for an exposure period of 4 h at ambient temperature of T_∞ = 28.5 °C and relative humidity RH_∞ = 31% at metabolic rate M = 1 met (58 W) at neutrality of steady state thermal comfort. Fig. 4 presents the simulated results of the modified current AUB model of (a) tympanic and body mean skin temperature, and (b) latent heat loss as a function of time in addition to the reported experimental data of Hardy and Stolwijk [7] and data of Salloum et al. model at the same conditions of the experiment [1]. Under steady state conditions, the mean skin and tympanic temperature predictions are closer to the measured values within ±0.3 °C than Salloum et al. [1]. The latent heat loss also agrees well with experimental measurement.

Cold-exposure experimental results of Raven and Horvath [52] for a nude body are compared with current model results for a cold step change in ambient temperature from 28.5 °C, 45% RH to 4.7 °C, 70% RH for a period of 2.5 h. Fig. 5 shows the measured [52], simulated temperatures of Salloum et al. [1], and current AUB model for a step change from 28 °C to 4.7 °C for (a) head skin temperature, (b) upper arm, and (c) thigh. The blood flow model has resulted in better agreement with experimental data in limbs skin temperature predictions.

The clothed human body model is validated against the published experimental data of Jones and Ogawa [45] and simulation results of Fu [37] and Salloum et al. [1]. The experimental data were reported for uniform environment at relative humidity of 50%, constant activity level of M = 1 met, and constant temperature of 21.1 °C (70 °F) continuing for a period of 60 min. The test was preceded by 45 min exposure to a cold environment of 4.4 °C. The fabric composition and the fabric physical and thermal parameters of each clothing layers (cotton, mixed cotton polyester, and polyester layers) used in the current comparison can be found in Refs. [1] and [45]. Fig. 6 shows the measured data of Jones and Ogawa [45], the predicted values of the current model and the model results of Salloum et al. [1] and of Fu [37] of (a) sensible and (b) latent heat losses to the environment from the clothed human body. When the cold fabric is suddenly exposed to hot environment at the same relative humidity, water vapor is adsorbed by the fabric raising its temperature and hence reducing sensible heat loss from the clothed human body. The current model simulation captures the transient effect and reproduces much better agreement with published experimental data of Jones and Ogawa than Salloum et al. [1] and the data of the more detailed and complex model of Fu [37].

A comparison of the clothed human model predictions against experimental data reported by Kakitsuba [53] is performed. The reported experiment protocol is similar to the one reported by

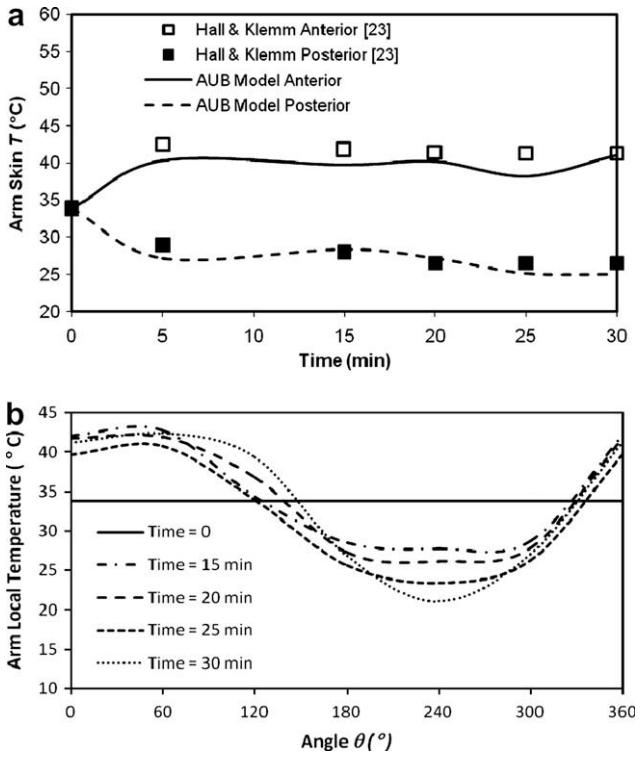

Fig. 9. A plot of (a) the predicted mean arm skin temperature for the anterior and posterior exposure for a period of 30 min as compared to experimental values [23] and (b) the angular variation of the arm skin temperature predicted by the model.

Jones and Ogawa [23]. The experimental data were for subjects wearing 100% cotton T-shirts and half shorts exposed to environment at 28 °C for a period of 30 min followed by a hot exposure to environment at 40 °C for a period of 1 h. Kakitsuba reported rectal and mean skin temperatures for the duration of the experiment, while the trunk and clothing temperatures were reported during the hot exposure period at 40 °C [1]. Fig. 7 shows the predicted (a) rectal and mean skin temperature and (b) the trunk skin and clothing temperatures by the current model, the Salloum et al. model [1], and by the experimental results of Kakitsuba [53]. The predicted rectal temperature, mean skin temperature and trunk skin temperatures are found to be consistent with the experimental measurements and in better agreement than Salloum et al. [1] model with a slight deviation in the predicted trunk clothing temperature from the experimental result due to the lumped approximation for the clothing element. Water vapor absorption under transient conditions due to water vapor accumulation in the microclimate could cause the clothing temperature to increase and then decrease approaching steady state condition. The model results show a similar increase/decrease in the trunk temperature to the experimental data of Kakitsuba [53] but with a smaller delay than Salloum et al. model [1]. Similar delays between experimental data and model were reported in literature [37] and attributed to the thermal load imposed by human test subjects when moving from pre-test condition chamber to the test chamber with a step change in temperature.

5.4. Asymmetric environment

Fanger et al. [54] conducted experiments in which they measured skin temperature in 14 locations of clothed subjects (clo-value = 0.6) seated in a room with a heated ceiling (2 m × 2 m) at height of 2.2 m above the floor with room air temperature range of 20.6–24.1 °C and radiant temperature asymmetry range from 0 to 23.6 °C corresponding to ceiling and room air temperature difference from 0 °C to 48 °C, respectively. Fig. 8a shows the reported measurements [54] and predicted values of current model of the skin temperature of the forehead, the calf, the foot, and the mean skin temperature as a function of radiant temperature asymmetry due to the hot ceiling. Fig. 8b shows the corresponding predictions of local temperature angular variation of the calf segment at radiant temperature asymmetry ΔT_{pr} of 0 °C, 5 °C, and 15 °C. The model predicts well the skin temperature with a maximum error of 0.5 °C in the mean skin temperature. At radiation asymmetry of 15 °C, the maximum local skin temperature difference of the calf reaches 4 °C. The segmental temperatures of the forehead, foot, and calf have shown smaller error.

Hall and Klemm [23] reported data transient experimental measurements from 27 experiments of 17 skin and rectal temperatures, heart rate, and evaporation rate during 30 min supine and 50 min prone exposure. The human body previously in neutral state is subjected to two radiative panels. The front panel is at 93.3 °C and the back panel at −6.7 °C. Fig. 9a shows the predicted

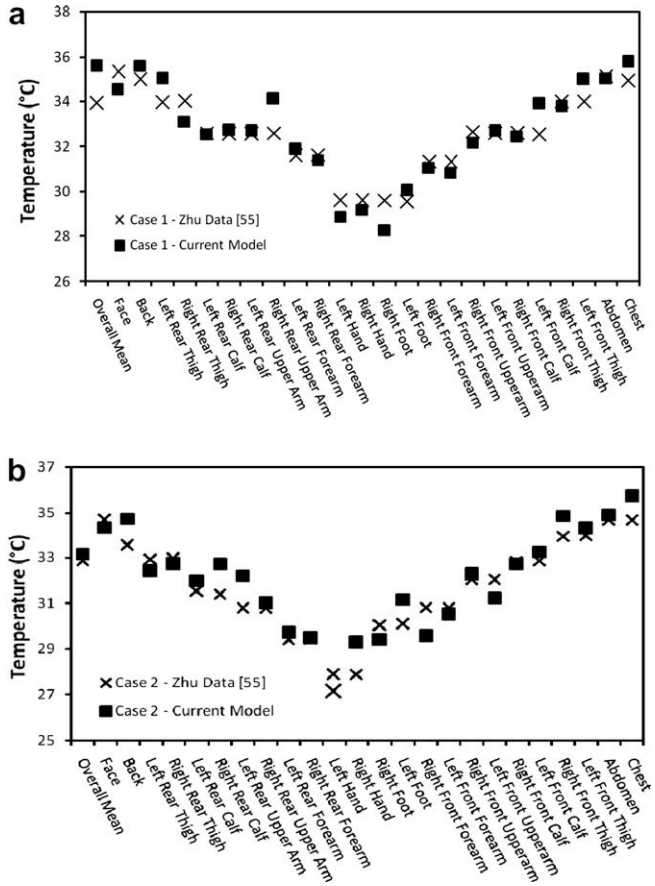

Fig. 10. The mean and local skin temperature for right and left parts and rear and front values of temperature of each part for (a) case 1 at frontal panel temperature of 8 °C and back panel temperature of 8 °C and (b) case 2 at frontal panel temperature of 4 °C and back panel temperature of 2 °C [55].

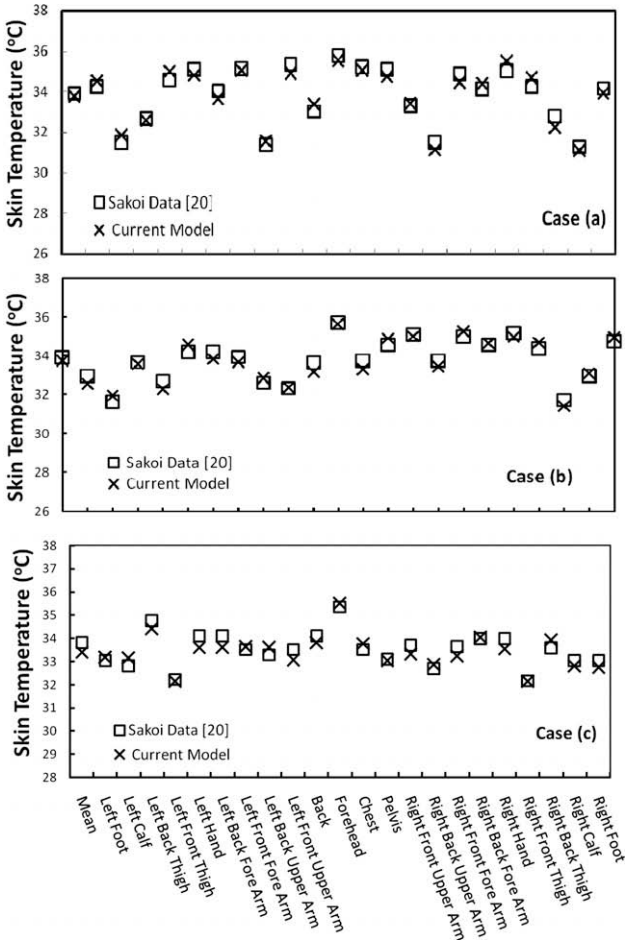

Fig. 11. The predicted mean skin temperature and segmental temperatures and reported experimental measurements of Sakoi et al. [20] in asymmetric radiative room for case (a) front/back, case (b) right/left, and case (c) upper/lower radiative panels at temperatures of 42 °C and 14 °C.

mean arm skin temperature for the anterior and posterior exposure for a period of 30 min as compared to experimental values [23] that reach 42 °C and 25 °C at the end of the exposure period. The predicted mean skin temperature of the anterior and posterior surfaces agree well with measured values with a maximum deviation less than ±0.5 °C for the anterior part and ±1.0 °C for the posterior part. The anterior minimum temperature is far below the anterior mean temperature because the perfusion blood rate is minimal in the corresponding sectors. The angular variation of the arm skin temperature predicted by the model is shown in Fig. 9b where the minimum and maximum skin temperatures reach values of 20 °C and 45 °C. The model captured the asymmetry in skin temperature to an acceptable degree of accuracy.

Zhu et al. [55] further developed Smith's 3D model [16] and simulated a seated person subjected to convective air at 8 °C at the floor level for two settings of the radiative panels' temperatures. The first case is at frontal panel temperature of 8 °C and back panel at 8 °C and the second case for a frontal panel at 4 °C and back panel at 2 °C. View factors for a seated person with room panels were obtained using our finite element model, and results of Zhu et al. [55] are reproduced using the current model. Fig. 10 shows the mean and local skin temperature for right and left parts and rear and front values of temperature of each part for (a) the uniform conditions of case 1 and (b) the asymmetric environment of case 2. The AUB model has captured the small asymmetry in skin temperature and agreed well with Zhu et al. model results [55] with highest deviation of ±0.8 °C in extremities.

Sakoi et al. [20] have recently reported local skin measurements at 25 locations for a clothed seated human and local sensible heat losses under experimental conditions of anterior–posterior, right–left, and up–down asymmetric thermal environments created by radiation panels from 11.5 °C to 44.5 °C. The subjects were preconditioned for 30 min before being subject to the radiative panels for 60 min at environment temperatures from 25.5 °C to 30 °C. For room environment at 28 °C, 40% relative humidity, panel temperatures of 42 °C and 14 °C, three room panel positions are considered in the comparison with current AUB model for case (a) front/ back, case (b) right/left, and case (c) upper/lower panels with respect to a seated subject in the middle of the room. Fig. 11 shows the predicted mean skin temperature and segmental temperatures and reported experimental measurements of Sakoi et al. [20] in asymmetric radiative room for case (a) front/back, case (b) right/left, and case (c) upper/lower radiative panels at temperatures of 42 °C and 14 °C. Fig. 12 shows the corresponding mean sensible and latent heat loss as predicted by the AUB bioheat current model and measured values reported by Sakoi et al. [20]. The bioheat model agreed well with the experimentally reported data on local and mean skin temperatures in asymmetric conditions and the corresponding heat loss from the human body.

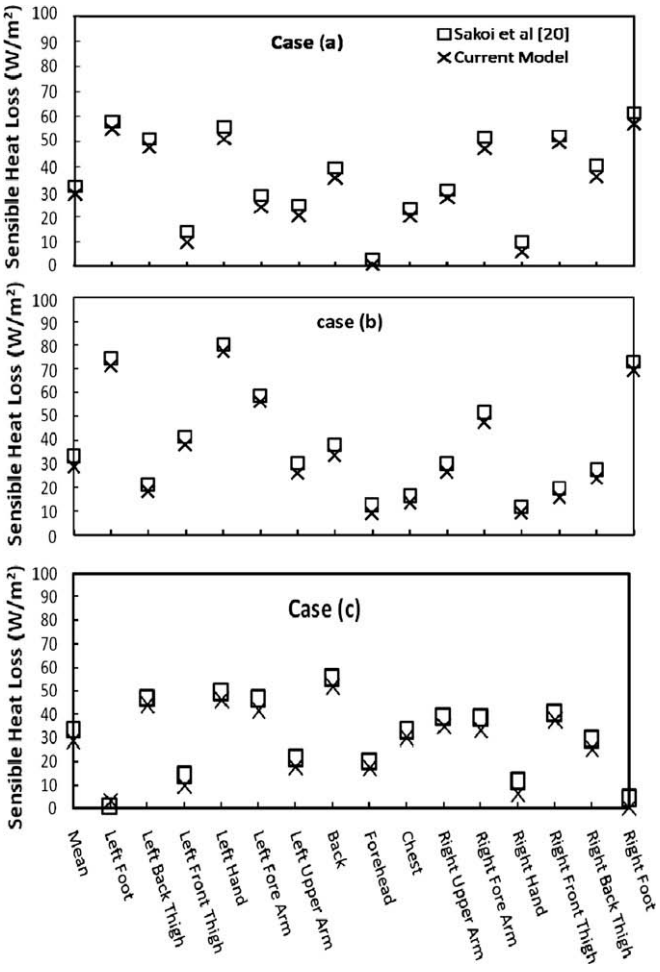

Fig. 12. The mean sensible and latent heat loss as predicted by the AUB bioheat current model and measured values reported by Sakoi et al. [20] for the cases (a), (b), and (c).

6. Conclusions

A human body bioheat model is developed from the previous AUB model to account for asymmetry. The modified model includes improvements in the circulatory system. The model was validated against lumped models, reported experimental data in transient and non-uniform radiative environments, and other asymmetric models for nude and clothed subjects and the results were consistent and agreed better with experimental data than the Salloum et al. model predictions [1]. The AUB model is able to predict the heat gains/losses at accuracy of less than 6% and with an accuracy of ±0.35 °C for mean skin temperature values.

Future work will address adding digits (fingers and toes) to the model to adapt the model for use in thermal sensation and thermal comfort studies in extreme environmental conditions.

Acknowledgements

The financial support of the Lebanese National Council for Scientific Research and of the Qatar Chair in Energy Studies Endowment Fund is greatly acknowledged.

References

[1] M. Salloum, N. Ghaddar, K. Ghali, A new transient bio-heat model of the human body and its integration to clothing models, Int. J. Therm. Sci. 46 (4) (2007) 371–384.
[2] A.P. Avolio, Multi-branched model of the human arterial system, Med Biol. Eng. Comp. 18 (1980) 709–718.
[3] M.S. Olufsen, C.S. Peskin, W.Y. Kim, E.M. Pedersen, A. Nadim, J. Larsen, Numerical simulation and experimental validation of blood flow in arteries with structured tree outflow conditions, Ann. Biomed. Eng. 28 (11) (2000) 1281–1299.
[4] H.H. Pennes, Analysis of tissue and arterial blood temperature in the resting human forearm, J. Appl. Phys. 1 (1948).
[5] S. Weinbaum, L. Jiji, Theory and experiment for the effect of vascular temperature on surface tissue heat transfer – part 1: anatomical foundation and model conceptualization, ASME J. Biomech. Eng. 106 (1984) 246–251.
[6] A.P. Gagge, A two node model of human temperature regulation in FORTRAN, in: J.F. Parker, V.R. West (Eds.), Bioastronautics Data, second ed., Washington, DC, 1973.
[7] J.A.J. Stolwijk, J.D. Hardy, Temperature regulation in man: a theoretical study, Pflügers Archiv. Ges. Physiol. 291 (1966) 129–162.
[8] J.A.J. Stolwijk, Mathematical model of thermoregulation, Physiological and Behavioral Temperature Regulation, Charles C. Thomas Publishing Company, Illinois, 1970.

[9] E.H. Wissler, Mathematical simulation of human thermal behavior using whole body models, Heat Mass Transfer in Medical Biology, Plenum Press, New York, 1985.
[10] C.H. Wyndham, A.R. Atkins, A physiological scheme and mathematical model of temperature regulation in man, Pfulgers Archiv. 303 (1968) 14–30.
[11] C. Huizenga, Z. Hui, A model of human physiology and comfort for assessing complex thermal environments, Build. Environ. 36 (2001) 691–699.
[12] S. Tanabe, K. Kobayashi, J. Nakano, Y. Ozeki, M. Konishi, Evaluation of thermal comfort using combined multi-node thermoregulation (65MN) and radiation models and computational fluid dynamics (CFD), Energy Build. 34 (2002) 637–646.
[13] D. Fiala, K.J. Lomas, M. Stohrer, Computer predictions of human thermoregulatory and temperature responses to a wide range of environment conditions, Int. J. Biometeorol. 45 (2001) 143–159.
[14] C. Huizenga, H. Zhang, E. Arens, D. Wang, Skin and core temperature response to partial- and whole-body heating and cooling, J. Therm. Biol. 29 (2004) 549–558.
[15] E. Arens, H. Zhang, C. Huizenga, Partial- and whole-body thermal sensation and comfort. Part II: Non-uniform environmental conditions, J. Therm. Biol. 31 (2006) 60–66.
[16] C.E. Smith, Ph.D. Thesis, A transient three-dimensional model of the thermal system, Kansas State University, 1991.
[17] E.Z.E. Conceição, M.M.J.R. Lúcio, T.M.C. Lourenço, A.I.P.V. Brito, Evaluation of thermal comfort in slightly warm ventilated spaces in non-uniform environments, HVAC R Res. 12 (3) (2006) 451–475.
[18] S.M. Frank, N.R. Srinivasa, C.F. Bulcao, D.S. Goldstein, Relative contribution of core and cutaneous temperatures to thermal comfort and autonomic responses in humans, J. Appl. Physiol. 86 (5) (1999) 1588–1593.
[19] F. Bauman, A. Baughman, G. Carter, E. Arens, A field study of PEM (Personal Environmental Module) performance in Bank of America's San Francisco Office Buildings, CEDR, University of California, Berkeley, 1998.
[20] T. Sakoi, T. Kazuyo, K. Shinsuke, R. Ooka, D. Song, S. Zhu, Thermal comfort, skin temperature distribution, and sensible heat loss distribution in the sitting posture in various asymmetric radiant fields, Build. Environ. 42 (2007) 3984–3999.
[21] K. Ghali, N. Ghaddar, M. Salloum, Effect of stove asymmetric radiation field on thermal comfort using a multi-segmented bioheat model, Build. Environ. 43 (7) (2008) 1241–1249.
[22] P.O. Fanger, L. Banhidi, B.W. Olesen, Comfort limits for heated ceilings, ASHRAE Trans. 86 (1980) 141–156.
[23] J.F. Hall, F.K. Klemm, Thermoregulatory responses in disparate thermal environments, J. Appl. Physiol. 23 (4) (1967) 540–544.
[24] T. Mungchareon, E.H. Wissler, A new two-dimensional human thermal model, AICHE Symp. Ser. 85 (269) (1989) 394–399.
[25] A. Iyoho, T. Jang, S. Nair, Human thermal model with extremities for asymmetric environments, in: Proceedings of the 2004 American Control Conference, Boston, MA, June 30–July 2, 2004, pp. 4366–4371.
[26] B.O. Fanger, Thermal Comfort Analysis and Applications in Engineering, McGraw Hill, New York, 1982.
[27] U. Gross, K. Spindler, E. Hahne, Shapefactor-equations for radiative heat transfer between plane rectangular surfaces of arbitrary position and size with parallel boundaries, Lett. Heat Mass Transfer 8 (3) (1981) 219–227.
[28] C.K. Krishnaprakas, View factor between inclined rectangles, AIAA J. Thermophys. Heat Transfer 11 (3) (1997) 480–482.
[29] N. Ghaddar, K. Ghali, M. Salam, Steady thermal comfort by radiant heat transfer: impact of heater position, Heat Transfer Eng. 27 (7) (2006) 29–40.
[30] Q. He, A three-dimensional human radiation model with finite element model, Ph.D. Thesis, Kansas State University, 1996.
[31] M. Olusfen, Modeling the Arterial System with Reference to an Anesthesia Simulator, Ph.D. Thesis, Rosklide University, 1998.
[32] M.S. Olufsen, A Structured tree outflow condition for blood flow in the larger systemic arteries, Am. J. Physiol., Heart. Circ. Physiol. 276 (1999) 257–268.
[33] M. Anliker, R.L. Rockwell, E. Ogden, Nonlinear analysis of flow pulses and shock waves in arteries, Z. Angew. Math. Phys. 22 (1971) 217–246.
[34] P. Segers, F. Dubois, D. DeWachter, P. Verdonck, Role and relevancy of a cardiovascular simulator, Cardiovas. Eng. 3 (1) (1998) 48–56.
[35] N. Stergiopulos, D.F. Young, T.R. Rogge, Computer simulation of arterial flow with applications to arterial aortic stenosis, J. Biomech. 25 (1992) 1477–1488.
[36] S. Stevens, W. Lakin, W. Goetz, A differentiable periodic function for pulsatile cardiac output based on heart rate stroke volume, Math. Biosci. (2002) 201–211.
[37] G. Fu, Ph.D. Thesis, A transient 3-D mathematical thermal model for the clothed human, Kansas State University, 1995.
[38] G. Havenith, Individualized model of human thermoregulation for the simulation of heat stress response, J. Appl. Phys. 90 (2000).
[39] R.G. Gordon, R.B. Roemer, S.M. Horvath, A mathematical model of the human temperature regulatory system – transient cold exposure response, IEEE Trans. Biomed. Eng. 23 (60) (1976) 434–444.
[40] A. Shitzer, R.C. Eberhart, Heat Transfer in Medicine and Biology: Analysis and Applications, Plenum Publishing Corporation, 1985.
[41] ASHRAE, Handbook of Fundamentals, American Society of Heating, Refrigerating and Air Conditioning Engineers, Atlanta, 2001.
[42] W.R. Milnor, Hemodynamics, second ed., Williams and Wilkins, 1989.
[43] X.L. Wang, Thermal comfort and sensation under transient conditions, Department of Energy Technology. Stockholm, The Royal Institute of Technology, 1994.
[44] B.W. Jones, Accurate modeling of heat and mass transport from the human body, in: 33rd Thermophysics Conference, 28 June–1 July, 1999, Norfolk, VA, USA.
[45] B.W. Jones, Y. Ogawa, Transient interaction between the human and the thermal environment, ASHRAE Trans. 98 (1993) 189–195.
[46] R.H. Howell, S. Suranarayana, Sizing of radiant heating systems. Part I: ceiling panels, ASHRAE Trans. 96 (1) (1990) 562–665 (AT-90-20-2 (3375, RP-394)).
[47] J.P. Holman, Heat Transfer, eighth ed., McGraw-Hill, New York, 1997 (Chapter 8).
[48] E.A. McCullough, B.W. Jones, P.E.J. Huck, A comprehensive database for estimating clothing insulation, ASHRAE Trans. 91 (1985) 29–47.
[49] E.A. McCullough, B.W. Jones, T. Tamura, A database for determining the evaporative resistance of clothing, ASHRAE Trans. 95 (1989) 316–328.
[50] C.J. Mills, I.T. Gabe, J.H. Gualt, P.T. Mason, J. Ross, E. Braunwald, Pressure-flow relationships and vascular impedance in man, Cardiovasc. Res. 4 (1970) 405–416.
[51] W.F. Ganong, Review of Medical Physiology, 11th ed., Lang Medical Publications, Los Altos, CA, 1983.
[52] P.R. Raven, S.M. Horvath, Variability of physiological parameters of unacclimatized males during a two-hour cold stress of 5 °C, Int. J. Biometeorol. 14 (1970) 309–320.
[53] N. Kakitsuba, Dynamic changes in sweat rates and evaporation rates through clothing during hot exposure, J. Therm. Biol. 29 (2004) 739–742.
[54] P.O. Fanger, L. Banhidi, B.W. Olesen, G. Langkilde, Comfort limits for heated ceilings, ASHRAE Trans. 86 (2) (1980) 141–156.
[55] S. Zhu, S. Kato, R. Ooka, T. Sakoi, Development of a computational thermal manikin applicable in a nonuniform thermal environment, HVAC R Res. 13 (4) (2007) 661–691.